Analysis of Internal Knee Forces Allows for the Prediction of Rupture Events in a Clinically Relevant Model of Anterior Cruciate Ligament Injuries

Ryo Ueno,*†‡ PT, PhD, Alessandro Navacchia,†‡ PhD, Nathaniel A. Bates,†‡§ PhD, Nathan D. Schilaty,†‡§ DC, PhD, Aaron J. Krych,†‡ MD, and Timothy E. Hewett,‖ PhD

Investigation performed at the Mayo Clinic, Rochester, Minnesota, USA

Background: A recently developed mechanical impact simulator induced an anterior cruciate ligament (ACL) rupture via the application of a combination of inverse dynamics–based knee abduction moment (KAM), anterior tibial shear force (ATS), and internal tibial rotation moment with impulsive compression in a cohort of cadaveric limbs. However, there remains an opportunity to further define the interaction of internal forces and moments at the knee and their respective influence on injury events.

Purpose: To identify the influence of internal knee loads on an ACL injury event using a cadaveric impact simulator.

Study Design: Controlled laboratory study.

Methods: Drop-landing simulations were performed and analyzed on 30 fresh-frozen cadaveric knees with a validated mechanical impact simulator. Internal forces and moments at the knee joint center were calculated using data from a 6-axis load cell recorded on the femur during testing. Kinetic data from a total of 1083 trials that included 30 ACL injury trials were used as inputs for principal component (PC) analysis to identify the most critical features of loading waveforms. Logistic regression analysis with a stepwise selection was used to select the PCs that predicted an ACL injury. Injurious waveforms were reconstructed with selected PCs in logistic regression analysis.

Results: A total of 3 PCs were selected in logistic regression analysis that developed a significant model ($P < .001$). The external loading of KAM was highly correlated with PC1 ($\rho < -0.8$; $P < .001$), which explained the majority (>69%) of the injurious waveforms reconstructed with the 3 selected PCs. The injurious waveforms demonstrated a larger internal knee adduction moment and lateral tibial force. After the ACL was ruptured, decreased posterior tibial force was observed in injury trials.

Conclusion: These findings give us a better understanding of ACL injury mechanisms using 6-axis kinetics from an in vitro simulator. An ACL rupture was correlated with an internal knee adduction moment (external KAM) and was augmented by ATS and lateral tibial force induced by an impact, which distorted the ACL insertion orientation.

Clinical Relevance: The ACL injury mechanism explained in this study may help target injury prevention programs to decrease injurious knee loading (KAM, ATS, and lateral tibial force) during landing tasks.

Keywords: ACL; landing; injury mechanism; principal component analysis

Anterior cruciate ligament (ACL) injuries are common in sports and may require surgical reconstruction, with a lengthy rehabilitation before athletes can return to sports in the majority of cases.[10] Only one-third of patients can return to their preinjury level of competitive sports by 12 months after surgery,[2] and one-fourth to one-third of athletes will suffer a second ACL injury within 2 years.[25] Therefore, prevention may be the most effective way to address these issues. ACL injury mechanisms have been extensively investigated to develop effective injury prevention programs.[1,11,20,32] Recent in vitro simulations of drop landings reported that combined external loads of knee abduction moment (KAM), anterior tibial shear force (ATS), and internal tibial rotation moment (ITR) coupled with an impulsive axial force increased ACL strain and produced clinically relevant ACL injuries.[5,7,14,15,17,27-29] The clinical relevance of those in vitro studies was corroborated with the location of tibial plateau bone bruises and ACL injuries that related to clinical observations of noncontact in vivo ACL injuries. However, it remains

The Orthopaedic Journal of Sports Medicine, 8(1), 2325967119893758
DOI: 10.1177/2325967119893758

unclear how these mixed loads result in internal knee forces or moments and what combination of internal knee kinetics causes an ACL injury.

These questions remain underinvestigated because internal forces cannot be measured during in vivo ACL injuries, which limits the understanding of the injury mechanism. Previous studies have investigated the interaction between external and internal loads with musculoskeletal models during a landing task.[26] However, these studies could not model the actual injury event. In vitro landing simulations can address these limitations, as the relationship between actual ACL ruptures and internal knee loads can be directly observed.

Principal component (PC) analysis (PCA) is an effective technique for the exploration of critical features in biomechanical data because it substantially reduces the number of variables needed to explain most of the variation between observations.[8] This method provides an objective characterization of waveform features that differ between participants. PCA of pooled biomechanical waveforms from multiple participants yields an orthogonal set of waveform features, called PCs, and a corresponding set of dimensionless PC scores for each participant.[13] Previous biomechanical studies have used PCA to detect differences in kinetic and kinematic waveforms through the interpretation of PCs between control and pathological groups.[9,30,33,34] This statistical method may clarify which features of internal knee kinetics are responsible for the reproduction of clinically relevant ACL injuries.

The purpose of this study was to explore the mechanical characterization that induces an ACL injury in cadaveric landing simulations using PCA and logistic regression analysis. According to previous studies, high ACL strain and ACL ruptures were observed with greater external loading in knee abduction.[7,14,15,17,27,29] This external loading condition induces an internal reaction moment in adduction. The hypothesis we tested was that the use of PCA and logistic regression analysis would describe the critical features of 6-axis kinetics that induce an ACL injury. Specifically, a larger internal knee adduction moment would be detected as a main factor of the high-risk kinetics that induce ACL injuries, and this high-risk kinetic feature would be found with the higher external loading condition of KAM.

METHODS

A total of 46 lower extremity cadaveric specimens were obtained from an anatomic donation program (Anatomy Gifts Registry). Specimens were between 14 and 50 years of age with no evidence of knee trauma, bone cancer, or knee surgery. Of these specimens, 6 were excluded from analysis because of structural weakness during setup ($n = 2$), substandard bone stiffness ($n = 1$), and equipment difficulties ($n = 3$). As the objective of this study required the precise identification of the ACL rupture event to conduct PCA, any specimens that experienced tissue failure that did not include an ACL rupture ($n = 5$), or for which the exact moment at which the rupture occurred was indeterminable from sensor data ($n = 2$), were excluded. Finally, 3 specimens were excluded because of minor deviations in the testing setup that did not influence ACL rupture outcomes but potentially could have confounded kinetic variables in $\geq$1 degrees of freedom (DOFs). Thus, there were 30 specimens that underwent the testing protocol and suffered an ACL rupture and were included in the final analysis (16 male [8 left/8 right]; 14 female [8 left/6 right]; mean age, 40.4 ± 8.8 years; mean weight, 80.7 ± 22.5 kg; mean height, 177.9 ± 49.5 cm).

All specimens were tested in the previously described mechanical impact simulator (Figure 1).[6] For experimental preparation, the muscle tissue of the hamstring and quadriceps was removed, leaving the tendinous tissue intact, which was secured into wire clamps. The femur was resected 20 cm proximal to the tibiofemoral joint line and inversely mounted on the mechanical impactor to apply an impulsive ground-reaction force by dropping a 34-kg weight onto the bottom of the foot. At the femoral fixture, a 6-DOF load cell (Omega160 IP65/IP68; ATI Industrial Automation) was secured to measure the forces and moments at the knee joint. The long axis of the femur was aligned with the vertical axis (z-axis in Figure 1A) of the 6-DOF load cell. The knee flexion angle was set to 25° to be consistent with the knee orientation at initial contact (IC) in young athletes landing from a drop height of 31 cm.[4] Pneumatic pistons (CG5LN40SV-100 and CG5LN50SV-100; SMC) mounted on the mechanical impactor were affixed to the tendon clamps to apply 450-N pretension to the quadriceps tendon and 225-N pretension to both hamstring tendon groups throughout testing. The magnitude of muscle forces was based on a previous report of maximum isometric voluntary contractions, and the force ratio between the quadriceps

*Address correspondence to Ryo Ueno, PT, PhD, Department of Orthopedic Surgery, Mayo Clinic, 200 1st Street SW, Rochester, MN 55905, USA (email: Ueno.Ryo@mayo.edu).
†Department of Orthopedic Surgery, Mayo Clinic, Rochester, Minnesota, USA.
‡Sports Medicine Center, Mayo Clinic, Rochester, Minnesota, USA.
§Department of Physiology and Biomedical Engineering, Mayo Clinic, Rochester, Minnesota, USA.
‖Department of Rehabilitation Sciences, University of Kentucky, Lexington, Kentucky, USA.
Final revision submitted September 20, 2019; accepted October 1, 2019.
One or more of the authors has declared the following potential conflict of interest or source of funding: The authors acknowledge funding from National Institutes of Health grants R01AR056259, R01AR055563, K12HD065987, and L30AR070273. A.J.K. has received consulting fees from Arthrex and Depuy Orthopaedics, has received royalties from Arthrex, and serves on the medical board of trustees for the Musculoskeletal Transplant Foundation. AOSSM checks author disclosures against the Open Payments Database (OPD). AOSSM has not conducted an independent investigation on the OPD and disclaims any liability or responsibility relating thereto.
Ethical approval was not sought for the present study.

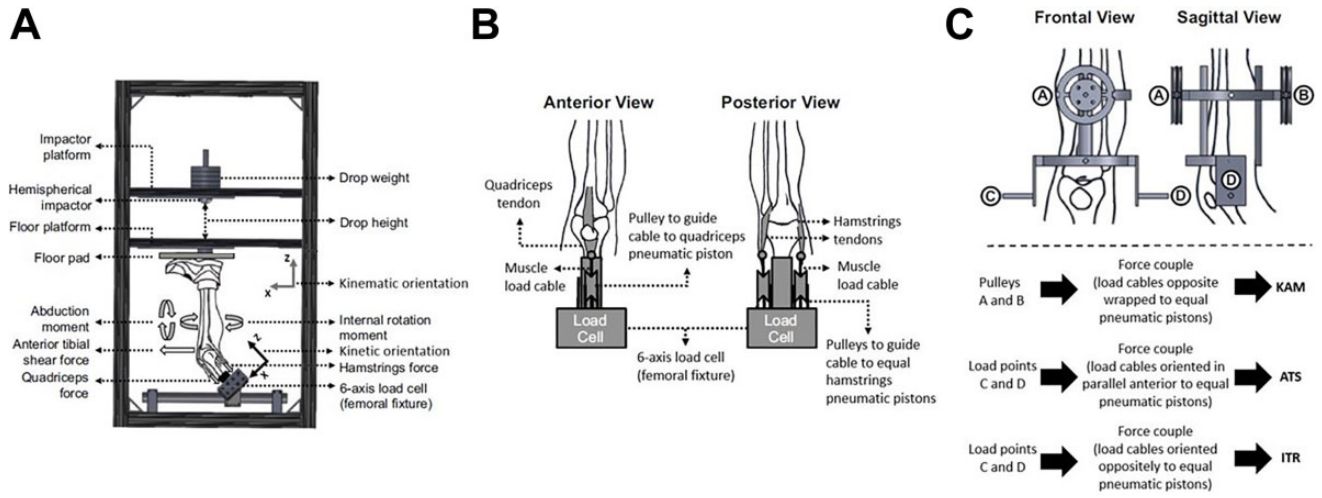

Figure 1. (A) Custom-designed mechanical impact simulator to produce clinically relevant anterior cruciate ligament (ACL) ruptures; (B) cable pulley system to deliver pneumatically actuated loads to the quadriceps and hamstring tendons; and (C) external fixation frame to deliver pneumatically actuated knee abduction moment (KAM), anterior tibial shear force (ATS), and internal tibial rotation moment (ITR) loads. Knee internal kinetic data were measured with a 6-axis load cell fixed to the femur. Its coordinate system was transformed to the knee joint center and rotated to align the *z*-axis to the long axis of the tibia. This figure has been adapted from Kiapour et al.[14]

and hamstring muscles was kept at 1:1.[6] Furthermore, Willigenburg et al[35] reported peak healthy quadriceps torque in female athletes to be approximately 155 N·m. As 30 to 35 cm is a common range for tibial length on a dynamometer, the estimated force to generate this torque would be calculated as around 442 to 517 N. Similarly, peak hamstring torque was approximately 77 N·m, which would have estimated a generating force of around 220 to 256 N.

Moreover, we affixed 5 additional pneumatic actuators (MQQTL40TN-100DM and CG5LN80SV-100; SMC) to apply external loads of ATS, KAM, and ITR to the knee joint. The exact loads were applied to both left- and right-side specimens in a randomized fashion. In this study, these acronyms will be used to refer to the external loading conditions applied by the pneumatic actuators. The external loads were based on in vivo motion analysis data previously collected from a cohort of 44 athletes (mean age, 23.3 ± 4.1 years; mean weight, 72.6 ± 13.9 kg; mean height, 172 ± 10 cm) who had performed drop vertical jump tasks.[6] The ATS, KAM, and ITR during the in vivo drop vertical jump task were calculated using inverse dynamics. For each loading condition, loading percentiles ranged from the 0th to 200th percentiles of the observed population of the in vivo cohort. Designations for these percentiles were baseline risk (<2nd percentile), low risk (~33rd percentile), moderate risk (~67th percentile), high risk (90th-100th percentile), and very high risk (200th percentile).

A total of 26 potential loading combinations were randomized and applied to each specimen (Table 1). Those external loads were increased until specimen failure was induced. A differential variable reluctance transducer (DVRT; LORD MicroStrain) was implanted onto the distal third of the anteromedial bundle of the ACL to record ACL strain. Because the DVRT data show unreasonable behavior only on a trial in which the ACL ruptures, the DVRT was also used to detect the ACL rupture trials.[7] The time of

TABLE 1
Combinations of Loading Conditions[a]

Condition	KAM, N·m	ATS, N	ITR, N·m
1	2.4	40	1.0
2	2.4	40	9.7
3	2.4	40	18.6
4	2.4	40	53.7
5	2.4	98	9.7
6	2.4	98	18.6
7	27.0	40	1.0
8	27.0	40	9.7
9	2.0	40	18.6
10	27.0	40	53.7
11	27.0	98	9.7
12	27.0	98	18.6
13	27.0	98	53.7
14	53.6	40	1.0
15	53.6	40	9.7
16	53.6	40	18.6
17	53.6	40	53.7
18	53.6	98	9.7
19	53.6	98	18.6
20	53.6	98	53.7
21	114.6	40	9.7
22	114.6	40	18.6
23	114.6	40	53.7
24	114.6	98	9.7
25	114.6	98	18.6
26	114.6	98	53.7

[a]ATS, anterior tibial shear force; ITR, internal tibial rotation moment; KAM, knee abduction moment.

peak ACL strain for ACL-intact trials was calculated to estimate the timing of an ACL rupture.[28]

All data were collected at 10 kHz and low pass filtered using a fourth-order zero-lag Butterworth filter at 50 Hz. The cutoff frequency of 50 Hz was chosen to leave the true signal unaffected based on spectral analysis, which calculates the width of the frequency band that contained 99% of the power of the signal performed on the 6-DOF load cell data.[36] The coordinate system of the 6-DOF load cell data was transformed to the knee joint center, and the vertical axis was aligned to the long axis of the tibia with a 25° rotation to obtain the internal forces and moments on the tibia respective to the femur (ie, reaction forces and moments on the tibia from the femur: anteroposterior force, mediolateral force, inferosuperior force, abduction-adduction moment, extension-flexion moment, and internal-external rotation moment). Data processing was performed using a custom MATLAB code (version 2017b; MathWorks).

Data from the 6-DOF load cell were collected for a total of 1083 trials, including 30 ACL injury trials, and was used as inputs for PCA to identify the most critical features of the loading waveforms in ACL injury trials. Before PCA, the 6-DOF load cell data were trimmed from 25 milliseconds before IC to 75 milliseconds after IC and resampled to 101 time points, so as to start before the impulsive force was applied and end after peak ACL strain was reached; this was done to reduce the PCs that resulted from the PCA.[15,16] The 6-DOF load cell data from left- and right-side specimens were separately used to conduct PCA processing because of the mechanical design of the impact simulator. The 6-DOF load cell was placed at the bottom of the mechanical impactor and connected to the frame.[6] A slight clockwise rotational oscillation of the 6-DOF load cell was visually identified in the frontal plane when the impact occurred, regardless of the specimen side. This potentially could affect the 6-DOF load cell data between sides, although there were no significant differences in ACL strain or failure type between left- and right-side specimens.[7,19]

The inputs for PCA consisted of 6-DOF waveform matrices composed of 525 trials × 606 data points and 558 trials × 606 data points for left- and right-side specimens, respectively. PCA was performed for each group after the data sets were normalized to the z score, a value divided by the standard deviation after subtracting the mean. Based on the broken-stick method,[12] 606 PCs were assessed for both the right- and left-side specimens. Of these, the 1st to 14th PCs were detected as significant and incorporated in logistic regression analysis for each side. Logistic regression analysis was performed to choose PCs that predict the ACL injury trials for left- and right-side groups separately. Waveforms that presented features of ACL injury trials were reconstructed using the PCs selected in logistic regression analysis as follows:

$$\hat{x} = \bar{x} + \sigma \sum_{k=1}^{n} u_k s_k,$$

where $\hat{x}$ (1 × 606) is the reconstructed waveform with n PCs selected in logistic regression analysis, $\bar{x}$ (1 × 606) is the mean waveform across all trials, σ (1 × 606) is the standard deviation to reconstruct unnormalized values from the z score, u_k (1 × 606) is a loading vector that is a coefficient variable showing the pattern of variance in the selected kth PC,[8] and s_k (1 × 606) is a high (95th percentile) or low (5th percentile) PC score for the kth PC, which indicates a high risk of ACL injury trials based on logistic regression analysis. The low- and high-risk kinetic waveforms were reconstructed on each DOF for left- and right-side specimens using the PCs selected in the corresponding logistic regression models (see the Appendix for the interpretation of each individual PC). Spearman rank-order correlation coefficients were used to determine the relationships between the external loading conditions and the PCs included in the logistic regression model. PCA and corresponding data processing were performed using a custom MATLAB code, while logistic regression analysis and calculations for the Spearman rank-order correlation coefficients were performed with JMP (version 14; SAS Institute). Statistical significance was set at $P < .05$.

RESULTS

For left-side specimens, the logistic regression model with 3 PCs was significant ($P < .001$) and presented 63% sensitivity, 98% specificity, and an area under the receiver operating characteristic curve of 0.86 (Figure 2A). The PCs that predicted an ACL injury were a low PC1 score ($P < .001$), high PC3 score ($P < .001$), and high PC9 score ($P = .005$). The scores for these 3 PCs during injury trials were significantly different ($P < .05$) from the corresponding scores during intact trials except for PC9 (Figure 3, A-C). PC1 explained 32.1% of the total variance of left-side specimens' 6-DOF kinetics (69.8% of the reconstructed waveform), and the PC1 score was negatively correlated with the KAM loading condition ($\rho = –0.814$; $P < .001$) (Table 2), meaning that high KAM trials presented low PC1 scores. The time of peak ACL strain for ACL-intact trials was 47.2 ± 7.8 milliseconds after IC.

For right-side specimens, the logistic regression model was significant ($P < .001$) and presented 79% sensitivity, 96% specificity, and an area under the receiver operating characteristic curve of 0.89 (Figure 2B). The included independent variables were a low PC1 score ($P < .001$), high PC5 score ($P = .003$), and low PC14 score ($P < .001$). The scores for these 3 PCs during injury trials were significantly different ($P < .05$) from the corresponding scores during intact trials (Figure 4, A-C). The KAM loading condition was significantly correlated with the PC1 score ($\rho = –0.827$; $P < .001$) (Table 2), which explained 33.1% of the total variance (81.9% of the reconstructed waveform). The time of peak ACL strain for ACL-intact trials was 41.1 ± 12.8 milliseconds after IC.

Anteroposterior force demonstrated an increase in ATS between 0 and 10 milliseconds after impact and posterior tibial force in the later phase (Figures 3D and 4D). Note that a taut ACL resists anterior tibial translation and induces posterior force on the tibia. High-risk waveforms showed a larger posterior tibial force before impact. After impact, both peak anterior and posterior forces were

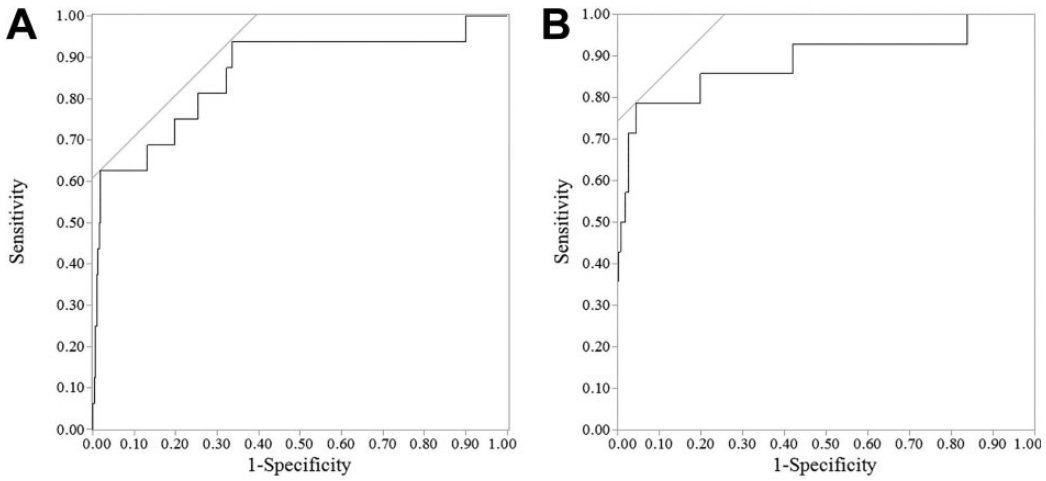

Figure 2. Receiver operating characteristic (ROC) curve from logistic regression analysis using principal components to predict anterior cruciate ligament injury trials for (A) left- and (B) right-side specimens. The areas under the ROC curve are 0.86 and 0.89 for left- and right-side specimens, respectively.

smaller in the high-risk waveforms compared with the low-risk waveforms. Both left- and right-side specimens presented a large lateral tibial force for high-risk waveforms (Figures 3E and 4E). Inferosuperior force in the high-risk waveforms showed a smaller compressive force compared with the low-risk waveforms for both left- and right-side specimens (Figures 3F and 4F).

The impact induced an internal adduction moment for left-side specimens and an abduction moment for right-side specimens (Figures 3G and 4G). This internal moment was a reaction force on the tibia from the femur. The high-risk waveforms showed a larger internal adduction moment before and after impact. The extension-flexion moment showed an internal flexion moment immediately after impact and then turned into an internal extension moment (Figures 3H and 4H). The high-risk waveforms demonstrated a smaller internal extension moment from 20 to 50 milliseconds after impact. For the internal-external rotation moment, the impact induced an external tibial rotation moment on the tibia for left-side specimens and ITR for right-side specimens. The difference between high- and low-risk waveforms was smaller than what was observed in the other DOFs (Figure 3I and 4I).

DISCUSSION

PCA was performed on 6-DOF knee kinetics measured in a cadaveric model that produced clinically relevant ACL injuries. Our primary hypothesis was that PCA would detect a larger internal knee adduction moment as a risk of ACL injuries and that this high-risk kinetic feature would be found when a higher KAM was applied. Briefly, the knee kinetic features of ACL injury trials were a smaller peak ATS, smaller peak posterior tibial force, larger lateral tibial force, smaller compressive force, and larger knee adduction moment. These kinetic data were induced with higher magnitude loading conditions, especially with the KAM loading condition, and the a priori hypothesis was supported.

In this study, PCA was used to identify the critical features that systematically describe the variability in knee kinetic data across simulated landing trials. PC scores from the significant modes of variation were used as independent variables for logistic regression analysis to isolate the kinetic features predictive of ACL injury trials. As reported in previous studies,[7,14,15,17,27,29] an ACL injury was associated with externally applied KAM loading. The present study enhanced our understanding of the injury mechanism associated with a large KAM by showing the features of 6-DOF internal knee loads in the clinically relevant ACL injury, which to our knowledge has not been done before. In particular, a larger internal lateral tibial force in ACL injury trials has never been reported in previous studies.

The effects of external loading conditions on injurious kinetics were largely consistent in left- and right-side specimens. The internal ATS that immediately followed impact was motivated by the sudden increase in compressive force caused by the impact, which produced a contact force on the tibia that was partially directed anteriorly because of the posterior tibial slope.[21,22] The increased internal ATS tensioned the ACL, which produced the internal posterior tibial force that was observed between 25 and 50 milliseconds after IC (Figures 3D and 4D). The larger internal posterior force before impact indicates that the pneumatically applied external loads tensioned the ACL in the injury trials more than intact trials before impact (Figure 5). This interpretation is supported by the correlation between KAM and PC1 (the high-risk waveform was mostly derived from PC1). A large KAM increases the contact force on the posterior part of the lateral tibial plateau, where the posterior slope is steeper (the slope angle is not constant; it becomes steeper on the

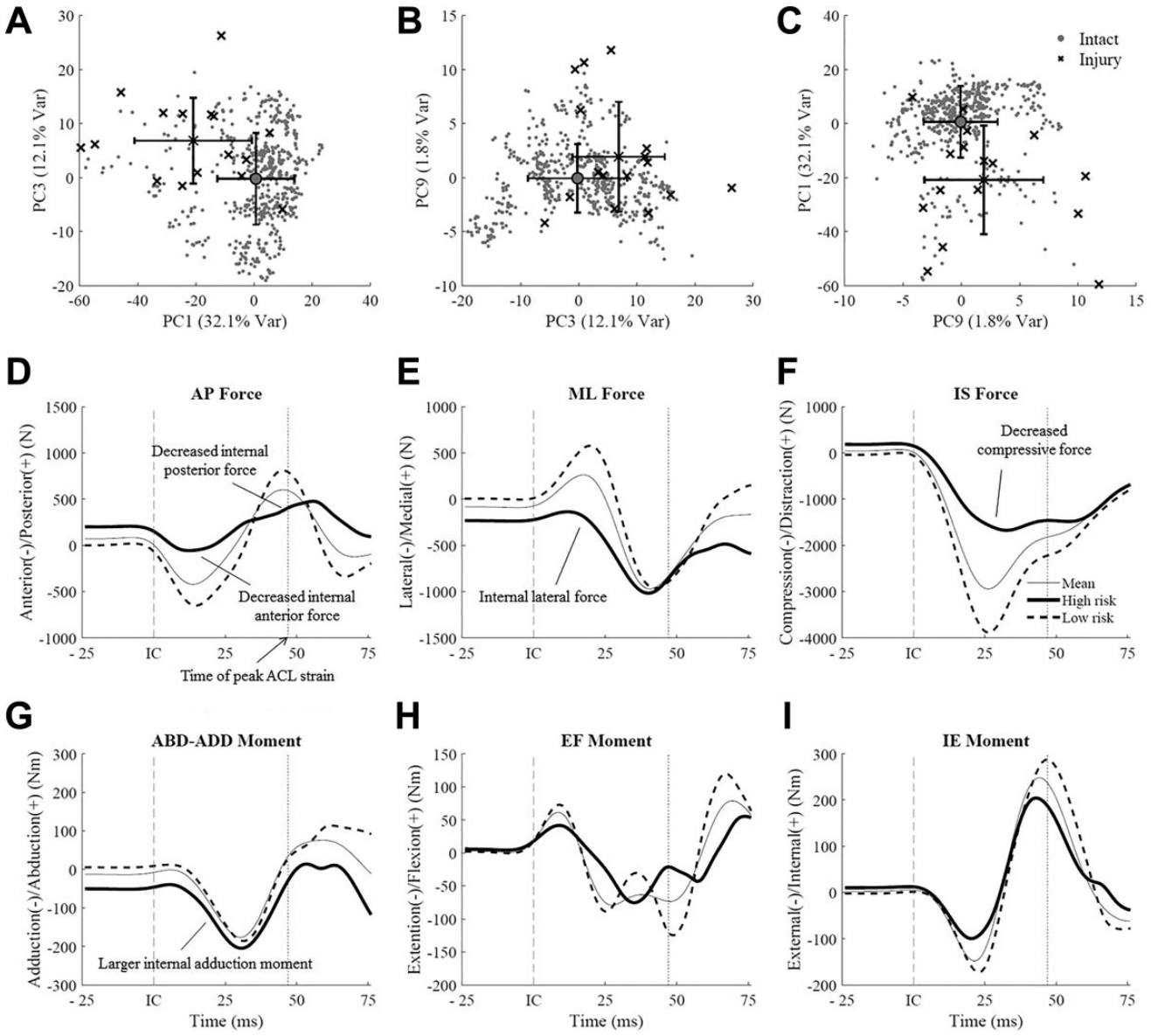

Figure 3. Left-side specimens. (A-C) Scatter plots comparing principal components (PCs) selected in logistic regression analysis between intact (dot) and injury trials (x) (A: PC1 vs PC3; B: PC3 vs PC9; C: PC9 vs PC1). The scores for these 3 PCs during injury trials were significantly different from the corresponding scores during intact trials except for PC9. The axis labels indicate the percentage of variance explained by each PC. (D-I) Mean (thin), high-risk (thick), and low-risk (dashed) kinetic waveforms reconstructed using the same 3 PCs. See the Appendix for a visual reconstruction of the waveform from a single PC and its related interpretation. ABD-ADD, abduction-adduction; ACL, anterior cruciate ligament; AP, anteroposterior; EF, extension-flexion; IC, initial contact; IE, internal-external rotation; IS, inferosuperior; ML, mediolateral.

posterior aspect of the tibia), exacerbating the effect of the posterior slope.[23] The decrease in peak internal posterior tibial force observed further from impulse delivery can be attributed to an ACL rupture, which occurred around 45 milliseconds after IC and removed the ligament-provided posterior pull on the tibia. These results indicated that a part of the force in the ACL was produced by the internal ATS induced by the impulsive compressive force on the posterior tibial slope (Figure 5). This finding explains the mechanical contribution of high-impact forces to ACL injuries.

For mediolateral force, there was a large internal lateral tibial force before and after impact for the high-risk waveforms (Figures 3E and 4E). This result was consistent with a previous study that demonstrated that compressive force induced medial translation of the femur relative to the tibia (ie, lateral tibial translation relative to the femur).[22] To our knowledge, there is little evidence related to the effect of

TABLE 2
Spearman Correlations Between External Loading Conditions and Principal Components (PCs) Selected in Logistic Regression Analysis[a]

	KAM		ATS		ITR	
	ρ	*P*	ρ	*P*	ρ	*P*
Left-side specimen						
PC1	–0.814	<.001	–0.382	<.001	–0.390	<.001
PC3	0.213	<.001	0.175	<.001	0.185	<.001
PC9	–0.076	.081	–0.169	<.001	–0.177	<.001
Right-side specimen						
PC1	–0.827	<.001	–0.376	<.001	–0.396	<.001
PC5	0.158	<.001	0.111	.009	0.158	<.001
PC14	–0.134	.002	0.009	.831	–0.017	.684

[a]ATS, anterior tibial shear force; ITR, internal tibial rotation moment; KAM, knee abduction moment.

internal lateral tibial force on ACL strain. Woo et al[37] indicated that mediolateral alignment of the tibia relative to the femur affected the ultimate load of the ACL in a tensile test. Specifically, when the tibia translates laterally and posteriorly relative to the femur, the anatomic angle of the ACL insertion on the bone is distorted and results in lower ultimate loads and higher rates of failure at the insertion, compared with when the ACL is tensioned along with the long axis of the ACL. The failure site in the present study primarily occurred on the femoral side, which is consistent with clinical populations.[7] The higher internal lateral tibial force may distort the femoral insertion of the ACL and induce ACL injuries under a lower internal ATS (Figure 5). This distorted condition was likely caused by high KAM loading, as indicated by the significant correlations between PC1 and the KAM loading condition (Table 2).

Notch impingement with an internal lateral tibial force would be another mechanism to increase ACL loads. However, notch impingement occurs with knee abduction and external rotation.[24] KAM and ITR loads applied in this study would induce internal (as opposed to external) tibial rotation because of the posterior tibial slope on the lateral compartment.[18,23] Further, as noted in the literature on our methodology, notchplasty was performed on our specimens to remove bone tissue from the inner wall of the femoral notch and subsequently prevent impingement of the implanted DVRT.[6] These facts indicated that intercondylar notch impingement would have been an unlikely mechanism of ACL injuries in this study.

Inferosuperior force of the high-risk waveforms showed that ACL injury trials presented a smaller compressive force (Figures 3F and 4F). In the trials with a lower KAM, the leg was vertically aligned throughout testing and presented a higher compressive force. However, when a high KAM was applied, the knee was abducted, and the foot of the specimen slid laterally from the mounted position, which may have allowed some of the impact force to transfer to an external KAM rather than pure compressive force. This behavior would have resulted in decreased compressive forces. Although decreased compressive forces were observed in the injurious waveforms, all the ACL ruptures were induced under impulsive compression but not during the application of external loading. As a previous study reported, increased compressive forces induce higher ACL strain.[27] Articular cartilage possibly was deformed by compressive force that would bring tibial and femoral ACL insertions into closer proximity. However, 1.69 to 2.55 mm of cartilage thickness was reported in a previous study,[31] and the space shortening relative to the ACL length would be limited. This fact indicated that an ACL rupture was enhanced under KAM loading even with the decreased compressive force.

The impact increased internal adduction moment for left-side specimens and abduction moment for right-side specimens (Figures 3G and 4G). This side-to-side difference might be motivated by the oscillation of the 6-DOF load cell that was attached to the impact simulator frame. Although the 6-DOF load cell was rigidly suspended, its attachment point was designed to have rotational capability to adjust for specimen-specific tibial alignment during setup.[6] This feature could have induced some oscillation upon impact, as the load cell was not directly grounded to the floor. However, the high-risk waveforms presented consistent changes with respect to low-risk waveforms for the 2 sides. There was a larger adduction moment before impact because of high KAM loading and a larger internal adduction moment after impact for left-side specimens (smaller internal abduction moment for right-side specimens). The hypothesis that the high-risk waveforms generate a larger internal adduction moment was partially supported by the results. Internal knee adduction moment may result from contact forces on the lateral tibial plateau and medial collateral ligament force. Contact force on the lateral compartment induces anterior tibial translation and internal tibial rotation.[18] The injurious internal ATS can be enhanced via this mechanism.

ACL rupture events may have influenced the extension-flexion moment, as the internal posterior tibial force decreased after a rupture. Immediate anterior tibial translation was visually identified for ACL injury trials, which can induce an internal flexion moment (external extension moment) at the knee joint center and justify the decrease in the internal extension moment around the time of the rupture event (Figures 3H and 4H). The internal-external rotation moment showed smaller differences between high- and low-risk waveforms (Figures 3I and 4I). Inverted waveforms between left- and right-side specimens were observed for the internal-external rotation moment. This may be related to the mechanical design of 6-DOF load cell fixation to the mechanical impact simulator apparatus that invoked a clockwise oscillation upon impulse delivery. While the oscillation was consistent between limbs, the rotational orientation of the *z*-axis was opposite between left and right sides.

A limitation of this study was that constant muscle forces were applied throughout each simulation; therefore, the effect of varied muscle loading was not investigated. The mechanical impact simulator was designed to apply in vivo kinetics from a drop vertical jump task to in vitro simulations of a drop landing. Because there were no ACL

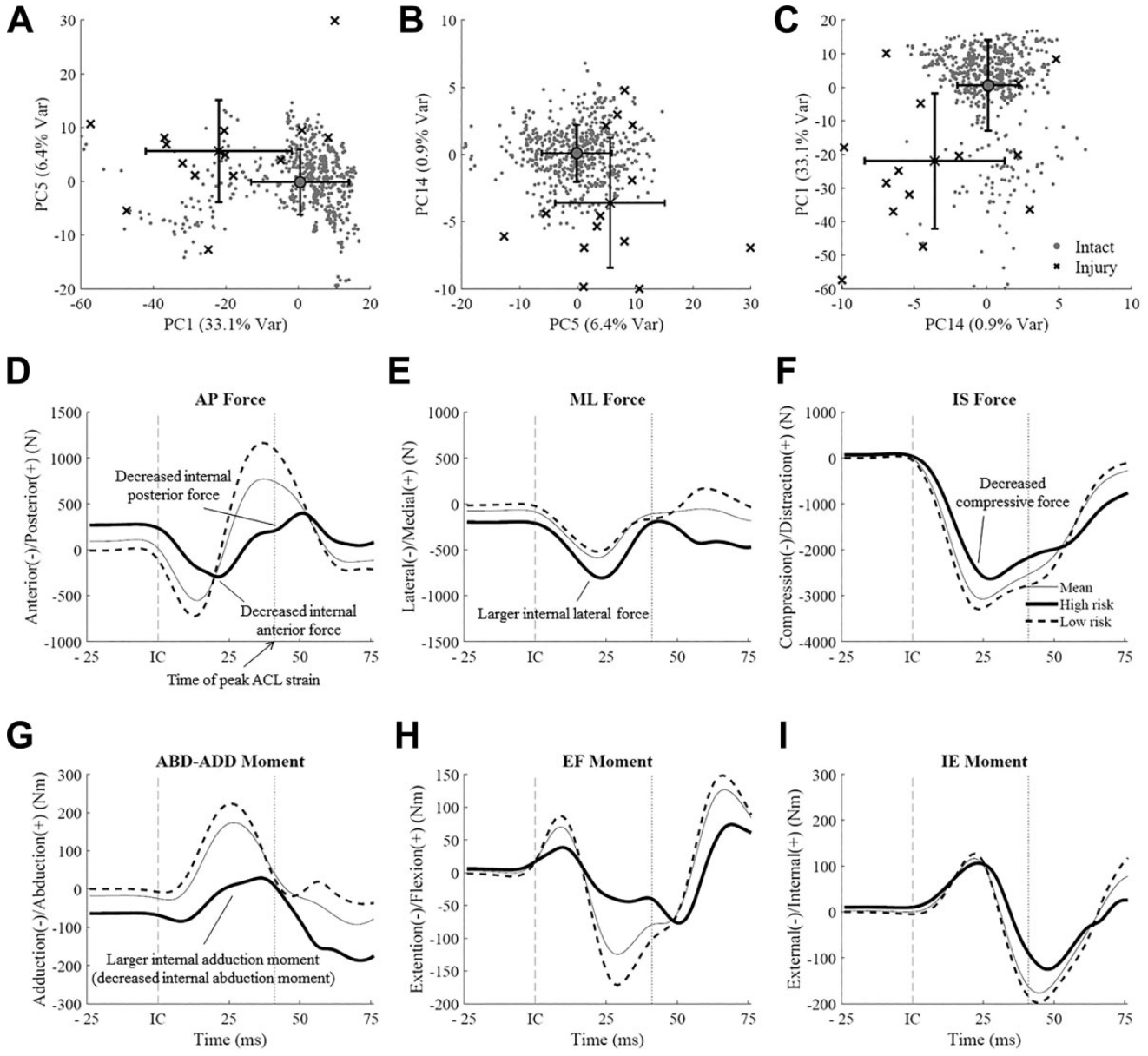

Figure 4. Right-side specimens. (A-C) Scatter plots comparing principal components (PCs) selected in logistic regression analysis between intact (dot) and injury trials (x) (A: PC1 vs PC5; B: PC5 vs PC14; C: PC14 vs PC5). The scores for these 3 PCs during injury trials were significantly different from the corresponding scores during intact trials. The axis labels indicate the percentage of variance explained by each PC. (D-I) Mean (thin), high-risk (thick), and low-risk (dashed) kinetic waveforms reconstructed using the same 3 PCs. See the Appendix for a visual reconstruction of the waveform from a single PC and its related interpretation. ABD-ADD, abduction-adduction; ACL, anterior cruciate ligament; AP, anteroposterior; EF, extension-flexion; IC, initial contact; IE, internal-external rotation; IS, inferosuperior; ML, mediolateral.

injuries during the in vivo drop vertical jump trials, the simulation of the muscle forces generated in vivo may serve to protect the ACL from kinetics that would otherwise be injurious. This concept will be explored in future work. In addition, the effect of varying drop weights was not tested in this study, as a previous study reported that larger compressive loads increase ACL strain.[27] This uniform weight, and consequent impulse force, may be another reason that a large compressive load was not detected in the injurious waveforms. Finally, the femur was rigidly fixed to the load cell, and this might have limited the ability of knee extension/flexion that influences ACL strain, although knee extension/flexion was not constrained.[3] Hyperextension has previously been shown to cause high strain/loading in the ACL, but our testing protocol did not evaluate this injury mechanism.

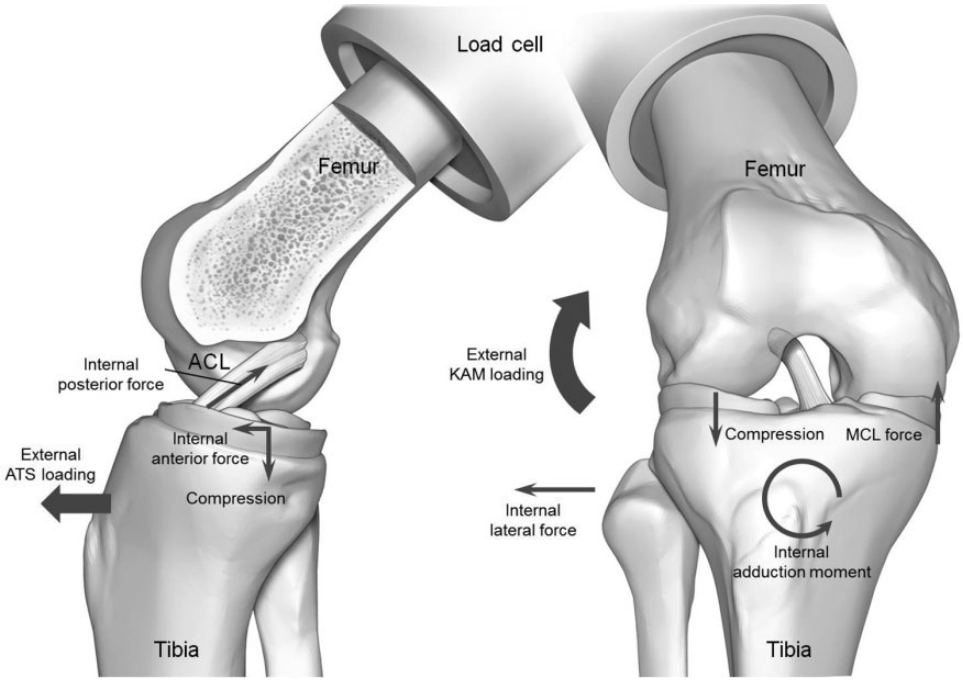

Figure 5. Schematic of injury mechanism. (Left) External loading of anterior tibial shear force (ATS) and compressive force on the posterior tibial slope induces an internal ATS and tensions the anterior cruciate ligament (ACL), which pulls the tibia posteriorly. (Right) External loading of knee abduction moment (KAM) induces an internal lateral tibial force, which may distort the femoral insertion of the ACL. KAM loads induce compression force on the lateral compartment and medial collateral ligament (MCL) tensile force that produce an internal knee adduction moment.

CONCLUSION

PCA was performed on 6-DOF knee kinetic data measured in a cadaveric model that produced clinically relevant ACL injuries. The waveforms reconstructed with the PCs selected by logistic regression analysis showed that ACL injury trials presented characteristic internal knee load features that were different compared with intact trials. Specifically, a smaller peak ATS, smaller peak posterior tibial force, larger lateral tibial force, smaller compressive force, and larger internal knee adduction moment were observed during ACL injury trials. These internal kinetic data were produced by larger external loading conditions, especially when a large KAM was applied. An ACL rupture was caused under ATS, and the rupture was facilitated by internal knee adduction moment and lateral tibial force that distorted the ACL at its femoral insertion site. The ACL injury mechanism explained in this study may help target injury prevention programs to decrease injurious knee loading (KAM, ATS, and lateral tibial force) during landing tasks.

ACKNOWLEDGMENT

The authors acknowledge support from the staff of the Materials and Structural Testing Core at the Mayo Clinic, the Biomechanics Research Laboratory at the Mayo Clinic, and the Sports Health and Performance Institute at The Ohio State University.

REFERENCES

1. Agel J, Rockwood T, Klossner D. Collegiate ACL injury rates across 15 sports: National Collegiate Athletic Association Injury Surveillance System data update (2004-2005 through 2012-2013). *Clin J Sport Med*. 2016;26(6):518-523.
2. Ardern CL, Webster KE, Taylor NF, Feller JA. Return to the preinjury level of competitive sport after anterior cruciate ligament reconstruction surgery: two-thirds of patients have not returned by 12 months after surgery. *Am J Sports Med*. 2011;39(3):538-543.
3. Bach JM, Hull ML, Patterson HA. Direct measurement of strain in the posterolateral bundle of the anterior cruciate ligament. *J Biomech*. 1997;30(3):281-283.
4. Bates NA, Ford KR, Myer GD, Hewett TE. Kinetic and kinematic differences between first and second landings of a drop vertical jump task: implications for injury risk assessments. *Clin Biomech (Bristol, Avon)*. 2013;28(4):459-466.
5. Bates NA, Schilaty ND, Nagelli CV, Krych AJ, Hewett TE. Multiplanar loading of the knee and its influence on ACL and MCL strain during simulated landings and noncontact tears. *Am J Sports Med*. 2019; 47(8):1844-1853.
6. Bates NA, Schilaty ND, Nagelli CV, Krych AJ, Hewett TE. Novel mechanical impact simulator designed to generate clinically relevant anterior cruciate ligament ruptures. *Clin Biomech (Bristol, Avon)*. 2017;44:36-44.
7. Bates NA, Schilaty ND, Nagelli CV, Krych AJ, Hewett TE. Validation of noncontact anterior cruciate ligament tears produced by a mechanical impact simulator against the clinical presentation of injury. *Am J Sports Med*. 2018;46(9):2113-2121.
8. Brandon SCE, Graham RB, Almosnino S, Sadler EM, Stevenson JM, Deluzio KJ. Interpreting principal components in biomechanics: representative extremes and single component reconstruction. *J Electromyogr Kinesiol*. 2013;23(6):1304-1310.

9. Federolf PA. A novel approach to study human posture control: "principal movements" obtained from a principal component analysis of kinematic marker data. *J Biomech*. 2016;49(3):364-370.
10. Griffin LY, Albohm MJ, Arendt EA, et al. Understanding and preventing noncontact anterior cruciate ligament injuries: a review of the Hunt Valley II meeting, January 2005. *Am J Sports Med*. 2006;34(9): 1512-1532.
11. Hewett TE, Bates NA. Preventive biomechanics: a paradigm shift with a translational approach to injury prevention. *Am J Sports Med*. 2017; 45(11):2654-2664.
12. Jackson DA. Stopping rules in principal components analysis: a comparison of heuristical and statistical approaches. *Ecology*. 1993;74(8): 2204-2214.
13. Jackson JE. *A User's Guide to Principal Components*. Hoboken, New Jersey: John Wiley & Sons; 1991.
14. Kiapour AM, Demetropoulos CK, Kiapour A, et al. Strain response of the anterior cruciate ligament to uniplanar and multiplanar loads during simulated landings: implications for injury mechanism. *Am J Sports Med*. 2016;44(8):2087-2096.
15. Kiapour AM, Quatman CE, Goel VK, Wordeman SC, Hewett TE, Demetropoulos CK. Timing sequence of multi-planar knee kinematics revealed by physiologic cadaveric simulation of landing: implications for ACL injury mechanism. *Clin Biomech (Bristol, Avon)*. 2014;29(1): 75-82.
16. Koga H, Nakamae A, Shima Y, et al. Mechanisms for noncontact anterior cruciate ligament injuries: knee joint kinematics in 10 injury situations from female team handball and basketball. *Am J Sports Med*. 2010;38(11):2218-2225.
17. Levine JW, Kiapour AM, Quatman CE, et al. Clinically relevant injury patterns after an anterior cruciate ligament injury provide insight into injury mechanisms. *Am J Sports Med*. 2013;41(2):385-395.
18. Matsumoto H. Mechanism of the pivot shift. *J Bone Joint Surg Br*. 1990;72(5):816-821.
19. McPherson AL, Bates NA, Schilaty ND, Nagelli CV, Krych AJ, Hewett TE. Ligament strain response between lower extremity contralateral pairs during in vitro landing simulation. *Orthop J Sports Med*. 2018; 6(4):2325967118765978.
20. Metcalf P, Scragg R, Davis P. Relationship of different measures of socioeconomic status with cardiovascular disease risk factors and lifestyle in a New Zealand workforce survey. *N Z Med J*. 2007; 120(1248):U2392.
21. Meyer EG, Haut RC. Anterior cruciate ligament injury induced by internal tibial torsion or tibiofemoral compression. *J Biomech*. 2008; 41(16):3377-3383.
22. Meyer EG, Haut RC. Excessive compression of the human tibiofemoral joint causes ACL rupture. *J Biomech*. 2005;38(11): 2311-2316.
23. Navacchia A, Bates NA, Schilaty ND, Krych AJ, Hewett TE. Knee abduction and internal rotation moments increase ACL force during landing through the posterior slope of the tibia. *J Orthop Res*. 2019; 37(8):1730-1742.
24. Park H-S, Ahn C, Fung DT, Ren Y, Zhang L-Q. A knee-specific finite element analysis of the human anterior cruciate ligament impingement against the femoral intercondylar notch. *J Biomech*. 2010; 43(10):2039-2042.
25. Paterno MV, Rauh MJ, Schmitt LC, Ford KR, Hewett TE. Incidence of second ACL injuries 2 years after primary ACL reconstruction and return to sport. *Am J Sports Med*. 2014;42(7):1567-1573.
26. Pflum MA, Shelburne KB, Torry MR, Decker MJ, Pandy MG. Model prediction of anterior cruciate ligament force during drop-landings. *Med Sci Sports Exerc*. 2004;36(11):1949-1958.
27. Quatman CE, Kiapour AM, Demetropoulos CK, et al. Preferential loading of the ACL compared with the MCL during landing: a novel in sim approach yields the multiplanar mechanism of dynamic valgus during ACL injuries. *Am J Sports Med*. 2014;42(1):177-186.
28. Schilaty ND, Bates NA, Krych AJ, Hewett TE. Frontal plane medial collateral ligament strain characteristics concurrent to anterior cruciate ligament failure. *Am J Sports Med*. 2019;47(9):2143-2150.
29. Schilaty ND, Bates NA, Nagelli C, Krych AJ, Hewett TE. Sex-based differences in knee kinetics with anterior cruciate ligament strain on cadaveric impact simulations. *Orthop J Sports Med*. 2018;6(3): 2325967118761037.
30. Schloemer SA, Thompson JA, Silder A, Thelen DG, Siston RA. Age-related differences in gait kinematics, kinetics, and muscle function: a principal component analysis. *Ann Biomed Eng*. 2017;45(3):695-710.
31. Shepherd DET, Seedhom BB. Thickness of human articular cartilage in joints of the lower limb. *Ann Rheum Dis*. 1999;58(1):27-34.
32. Shimokochi Y, Shultz SJ. Mechanisms of noncontact anterior cruciate ligament injury. *J Athl Train*. 2008;43(4):396-408.
33. Soares DP, de Castro MP, Mendes EA, Machado L. Principal component analysis in ground reaction forces and center of pressure gait waveforms of people with transfemoral amputation. *Prosthet Orthot Int*. 2016;40(6):729-738.
34. Watari R, Osis ST, Phinyomark A, Ferber R. Runners with patellofemoral pain demonstrate sub-groups of pelvic acceleration profiles using hierarchical cluster analysis: an exploratory cross-sectional study. *BMC Musculoskelet Disord*. 2018;19(1):120.
35. Willigenburg NW, McNally MP, Hewett TE. Quadriceps and hamstrings strength in athletes. In: Kaeding CC, Borchers JR, eds. *Hamstring and Quadriceps Injuries in Athletes*. New York: Springer; 2014: 15-28.
36. Winter DA. *Biomechanics and Motor Control of Human Movement*. 4th ed. Hoboken, New Jersey: John Wiley & Sons; 2009.
37. Woo SL, Hollis JM, Adams DJ, Lyon RM, Takai S. Tensile properties of the human femur-anterior cruciate ligament-tibia complex: the effects of specimen age and orientation. *Am J Sports Med*. 1991; 19(3):217-225.

APPENDIX

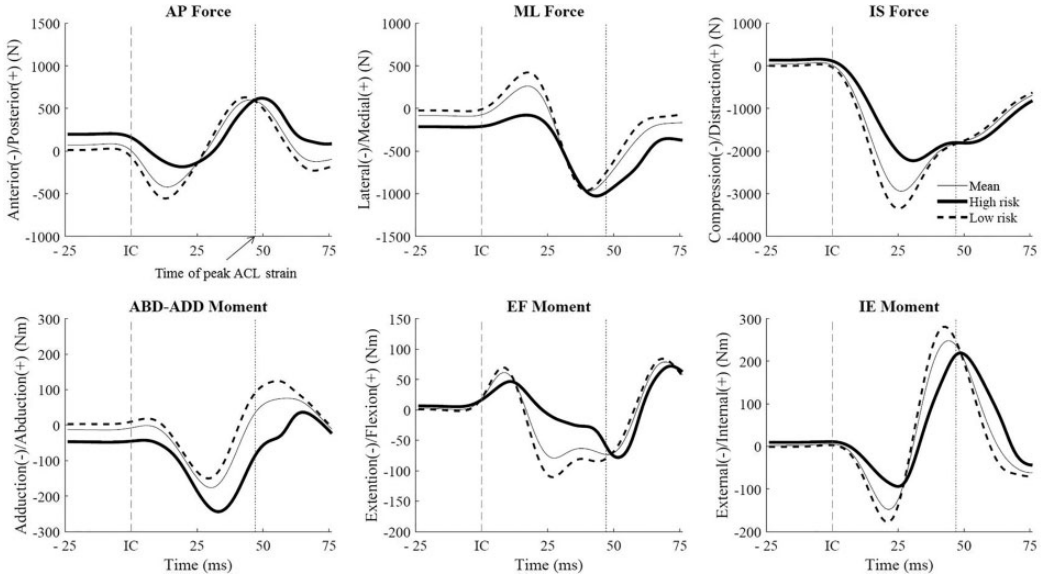

Figure A1. Mean (thin), high-risk (thick), and low-risk (dashed) kinetic waveforms reconstructed from left-side specimen PC1. Among the features of a reconstructed waveform using all of the 3 principal components, the high-risk waveform in PC1 shows a larger internal posterior tibial force before impact, decreased internal anterior tibial shear force immediately after impact, larger internal lateral tibial force before and immediately after impact, decreased compressive force, larger internal knee adduction moment throughout testing, and decreased internal knee extension moment around the time of the rupture event. The range of IE moments was also decreased in the high-risk waveform. Those kinetic features were induced under higher external loading conditions, especially knee abduction moment according to the results of Pearson correlations. However, the decreased rotation moment in the high-risk waveform was canceled out by integrating PC9. ABD-ADD, abduction-adduction; ACL, anterior cruciate ligament; AP, anteroposterior; EF, extension-flexion; IC, initial contact; IE, internal-external rotation; IS, inferosuperior; ML, mediolateral.

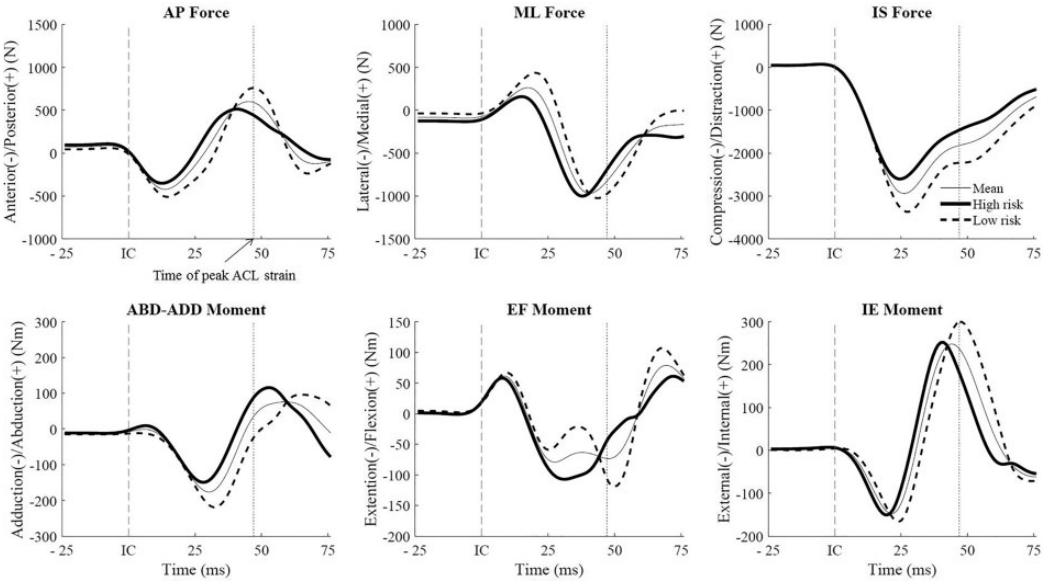

Figure A2. Mean (thin), high-risk (thick), and low-risk (dashed) kinetic waveforms reconstructed from left-side specimen PC3. The high-risk waveform reconstructed from PC3 was induced by higher external loading conditions that showed similar but faster waveforms compared with that of PC1 for AP force, ML force, and IS force. However, opposite waveform patterns were described for ABD-ADD moment, EF moment, and IE moment. Integrating those waveforms, the features of high-risk waveforms for forces were slightly enhanced and made faster, but the features for moments were diminished. In addition, the same feature of decreased internal posterior force around the time of the rupture event shown in Figure 3D can be found in this PC3. ABD-ADD, abduction-adduction; ACL, anterior cruciate ligament; AP, anteroposterior; EF, extension-flexion; IC, initial contact; IE, internal-external rotation; IS, inferosuperior; ML, mediolateral.

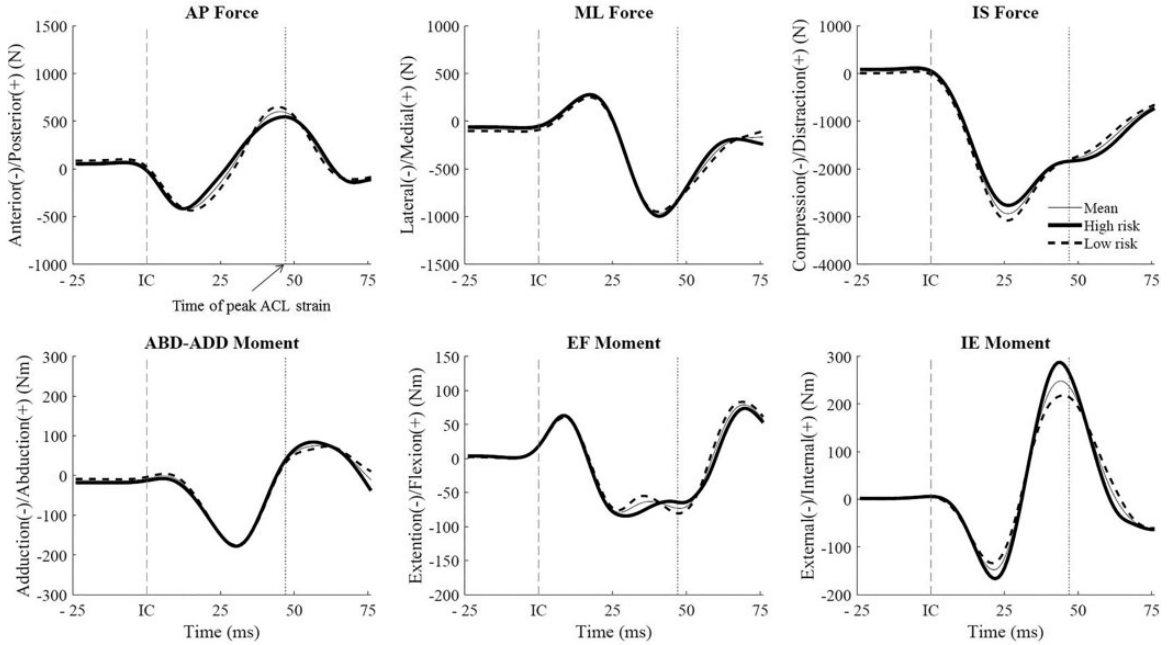

Figure A3. Mean (thin), high-risk (thick), and low-risk (dashed) kinetic waveforms reconstructed from left-side specimen PC9. Negative correlations between PC9 and external loading conditions explain that the high-risk waveform in PC9 was induced under lower external loading conditions because a high PC9 score was included in the logistic regression model. For the effect of external loading on IE moments, it is consistent with PC1 that higher external loading conditions decreased the range of IE moments. PC9 might be included in the logistic regression model to adjust the decreased IE moment in PC1 for the prediction of ACL injury trials. ABD-ADD, abduction-adduction; ACL, anterior cruciate ligament; AP, anteroposterior; EF, extension-flexion; IC, initial contact; IE, internal-external rotation; IS, inferosuperior; ML, mediolateral.

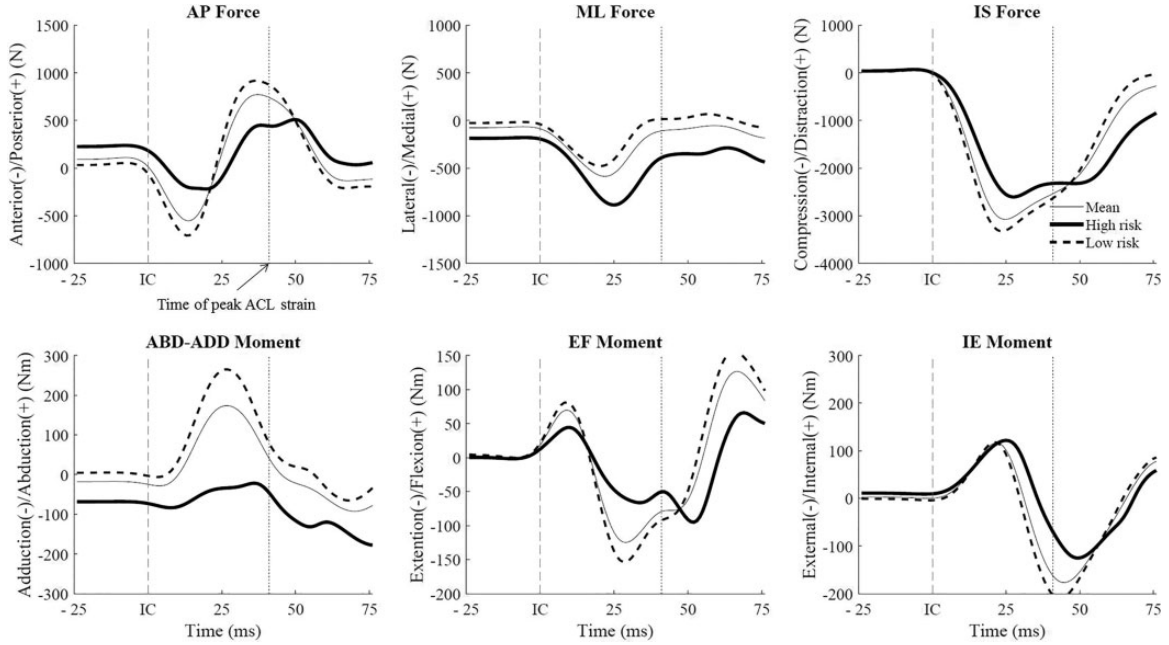

Figure A4. Mean (thin), high-risk (thick), and low-risk (dashed) kinetic waveforms reconstructed from right-side specimen PC1. PC1 explains 81.9% of the reconstructed waveforms from all of the 3 principal components. Similar to left-side specimens, higher external loading conditions, especially knee abduction moment, induced high-risk waveforms in PC1. ABD-ADD, abduction-adduction; ACL, anterior cruciate ligament; AP, anteroposterior; EF, extension-flexion; IC, initial contact; IE, internal-external rotation; IS, inferosuperior; ML, mediolateral.

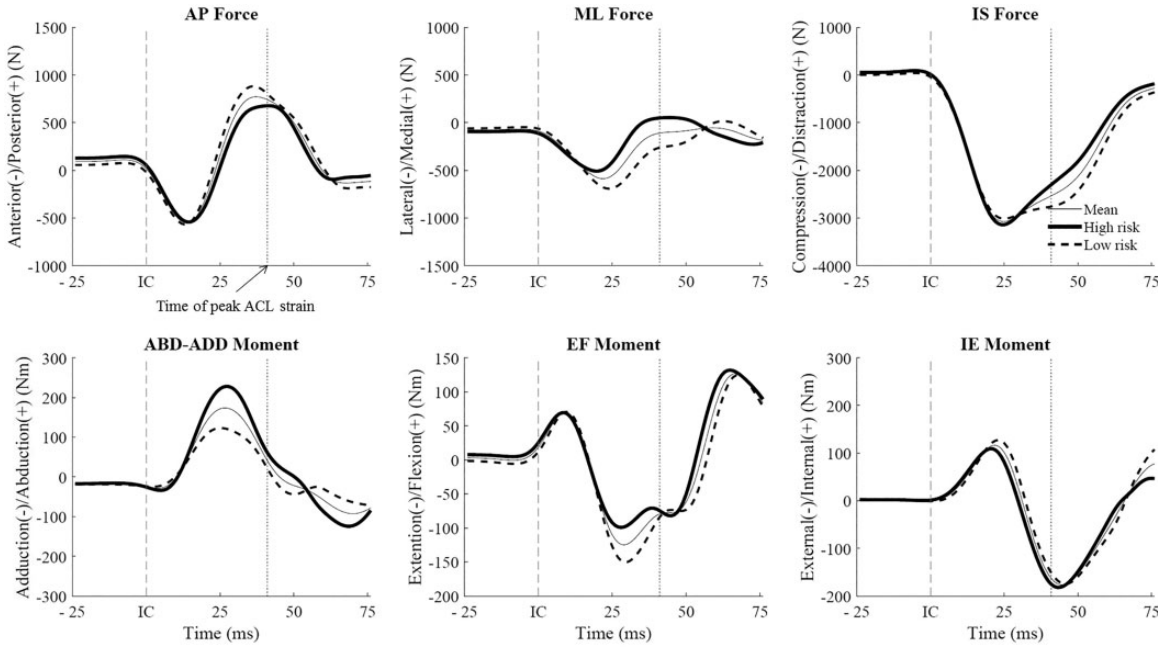

Figure A5. Mean (thin), high-risk (thick), and low-risk (dashed) kinetic waveforms reconstructed from right-side specimen PC5. The effect of PC5 on integrated waveforms was smaller compared with PC1. The main features of PC5 were a smaller internal lateral tibial force and larger internal knee abduction moment after impact that were opposite to the high-risk waveform in PC1. These features might be included in the logistic regression model to adjust the large internal lateral tibial force and small internal knee adduction moment in PC1 as in left-side specimen PC9. ABD-ADD, abduction-adduction; ACL, anterior cruciate ligament; AP, anteroposterior; EF, extension-flexion; IC, initial contact; IE, internal-external rotation; IS, inferosuperior; ML, mediolateral.

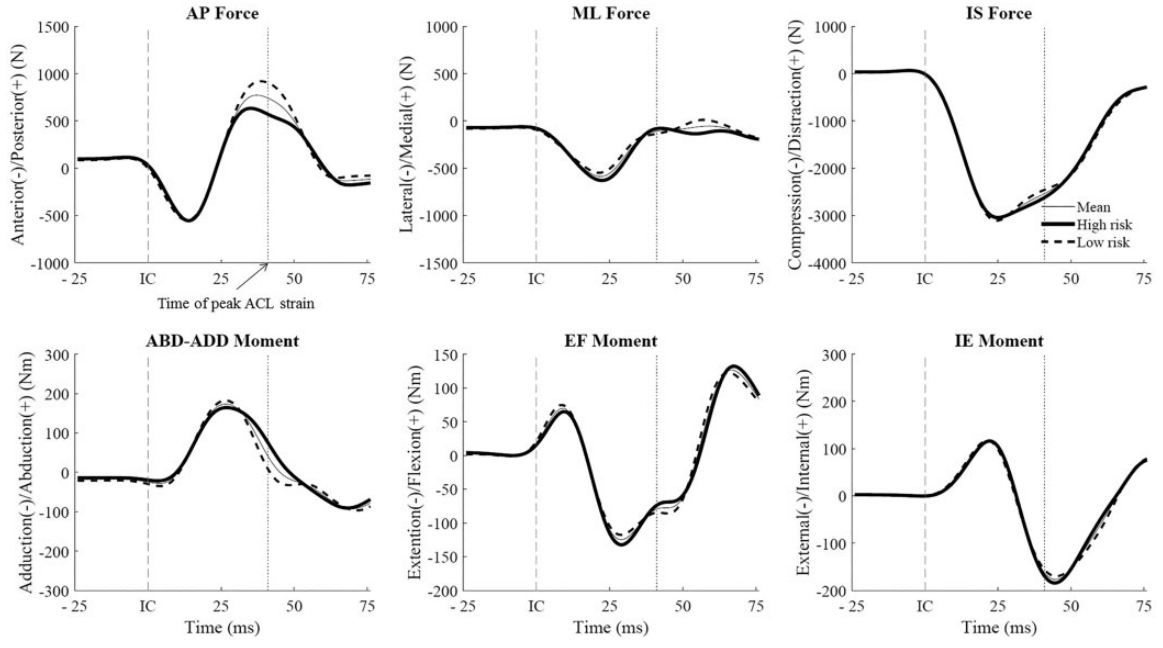

Figure A6. Mean (thin), high-risk (thick), and low-risk (dashed) kinetic waveforms reconstructed from right-side specimen PC14. The prime feature of PC14 was a decreased internal posterior tibial shear force around the time of the ACL rupture that enhanced the feature of high-risk waveforms in Figure 4D in the main text. ABD-ADD, abduction-adduction; ACL, anterior cruciate ligament; AP, anteroposterior; EF, extension-flexion; IC, initial contact; IE, internal-external rotation; IS, inferosuperior; ML, mediolateral.